Monthly Notices
of the
ROYAL ASTRONOMICAL SOCIETY

Mon. Not. R. Astron. Soc. **404,** 1005–1017 (2010) doi:10.1111/j.1365-2966.2010.16333.x

9C continued: results from a deeper radio-source survey at 15 GHz

E. M. Waldram,[1⋆] G. G. Pooley,[1] M. L. Davies,[1] K. J. B. Grainge[1,2] and P. F. Scott[1]

[1]*Astrophysics Group, Cavendish Laboratory, J J Thomson Avenue, Cambridge CB3 0HE*
[2]*Kavli Institute for Cosmology Cambridge, Madingley Road, Cambridge CB3 0HA*

Accepted 2010 January 11. Received 2009 December 10; in original form 2009 July 29

ABSTRACT

The 9C survey of radio sources with the Ryle Telescope at 15.2 GHz was set up to survey the fields observed with the cosmic microwave background telescope, the Very Small Array. In our first paper, we described three regions of the survey, constituting a total area of 520 deg^2 to a completeness limit of ≈25 mJy. Here we report on a series of deeper regions, amounting to an area of 115 deg^2 complete to ≈10 mJy and of 29 deg^2 complete to ≈5.5 mJy. We have investigated the source counts and the distributions of the 1.4 to 15.2 GHz spectral indices ($\alpha_{1.4}^{15.2}$) for these deeper samples. The whole catalogue of 643 sources is available online.

Down to our lower limit of 5.5 mJy, we detect no evidence for any change in the differential source count from the earlier fitted count above 25 mJy, $n(S) = 51(S/\mathrm{Jy})^{-2.15}\ \mathrm{Jy}^{-1}\ \mathrm{sr}^{-1}$.

We have matched both our new and earlier catalogues with the NRAO VLA Sky Survey (NVSS) catalogue at 1.4 GHz and selected flux-limited samples at both 15 and 1.4 GHz. As expected, we find that the proportions of sources with flat and rising spectra in the samples selected at 15 GHz are significantly higher than those in the samples selected at 1.4 GHz. In addition, for 15-GHz samples selected in three flux density ranges, we detect a significant shift in the median value of $\alpha_{1.4}^{15.2}$: the higher the flux densities the higher the proportions of sources with flat and rising spectra.

In our area complete to ≈10 mJy, we find five sources between 10 and 15 mJy at 15 GHz, amounting to 4.3 per cent of sources in this range, with no counterpart in the NVSS catalogue. This implies that, had we relied on NVSS for locating our sources, we could have missed a significant proportion of them at low flux densities.

Our results illustrate the problems inherent in using a low-frequency catalogue to characterize the source population at a much higher frequency and emphasize the value of our blind 15.2-GHz survey.

Key words: surveys – galaxies: evolution – cosmic microwave background – radio continuum: general.

1 INTRODUCTION

As explained in our first paper (Waldram et al. 2003, hereafter Paper I) , the 9C survey with the Ryle Telescope (RT) at 15.2 GHz was designed specifically as part of the observing strategy of the Very Small Array (VSA; Watson et al. 2003). Foreground radio sources are a major contaminant in the cosmic microwave background (CMB) observations of the VSA at 34 GHz, and the prime purpose of the 9C survey has been to provide a catalogue of radio sources in each of the VSA fields (Taylor et al. 2003; Cleary et al. 2005, 2008). This has meant that the positions of the 9C fields and their depth in different areas have been determined by the VSA observing programme. For the VSA compact array (ℓ = 150 to 800) we covered a total area of 520 deg^2 to a completeness limit of 25 mJy, but for the extended array (ℓ = 300 to 1500) and now the superextended array (ℓ = 600 to 2500) deeper surveying over some smaller regions has been required. It is these regions which are described here.

In addition to its specific application to the VSA observations, the 9C survey has proved to be of much wider interest. There have been other blind surveys at high radio frequencies, notably with the Australia Telescope Compact Array (ATCA) at 18 and 20 GHz (Ricci et al. 2004; Sadler et al. 2006; Massardi et al. 2008; Murphy et al. 2010), but 9C was the first such survey of any extent and is the only one to reach such low flux densities. It provides an important opportunity for exploring the radio-source population at high frequencies. Samples of 9C sources have been followed up with simultaneous multifrequency observations at 1.4, 4.8, 15.2, 22 and 43 GHz (Bolton et al. 2004), and there have been two further papers

⋆E-mail: e.m.waldram@mrao.cam.ac.uk

based on these data: Bolton et al. (2006a), which describes results from 5-GHz Multi-Element Radio-Linked Interferometer Network (MERLIN) and Very Long Baseline Array (VLBA) observations and Bolton et al. (2006b), which examines variability at 15.2 GHz.

As a blind survey at 15.2 GHz, 9C is particularly valuable in the study of source counts at high radio frequencies. Point sources are a significant foreground in the CMB observations of many instruments (e.g. *Planck*) and, even if the brighter sources can be identified and subtracted from the data, there remains the problem of residual confusion from the fainter, unsubtracted source population. This effect can be evaluated only from a knowledge of the source counts below the subtraction limit. Blind surveys at frequencies of 30 GHz and above are extremely problematical because of the small field of view of the available telescopes, so one approach has been to identify sources from a lower frequency survey, with a measured source count, and follow them up at the higher frequency. 9C, at 15.2 GHz, is comparatively close to the target frequencies and, therefore, has a considerable advantage over lower frequency surveys.

We have used this method to make empirical estimates of the source counts at higher frequencies (including those in the lower *Planck* bands) by taking the spectral index distributions from the Bolton data together with our known 15.2-GHz source count (Waldram et al. 2007). Comparison with the theoretical model of de Zotti et al. (2005) shows good agreement below 43 GHz, but at higher frequencies there is some divergence towards higher flux densities, indicating that our predictions imply fewer flat spectrum sources. However, the results of Sadler et al. (2008), who have made simultaneous observations with ATCA of a sample of sources at 20 and 95 GHz, do appear to confirm our own estimates of the count at 90 GHz in the common flux density range.

More recently, Mason et al. (2009) have made a 31-GHz survey of the fields of the Cosmic Background Imager (CBI; Mason et al. 2003) by following up known extragalactic sources from the NRAO VLA Sky Survey (NVSS) survey at 1.4 GHz (Condon et al. 1998). They have estimated the spectral index distribution from 1.4 to 31 GHz and hence the 31-GHz source count in the range 0.5 to 10 mJy, which has enabled them to make an assessment of the contribution of unresolved point sources to the CBI power spectrum. Our results here provide a useful comparison with their work.

Also, a subset of the sources in our present catalogue has now been followed up at 30 GHz with observations made using the 32-m Toruń telescope (Gawroński et al. 2009).

In this paper, we first explain the choice of fields and our methods of observation and data analysis, together with estimates of completeness and a description of the source catalogue (Sections 2, 3, 4 and 5). Section 6 presents the extended source counts. We then investigate the correlation of our source lists with the NVSS catalogue. In Section 7, we report the results and in Section 8 discuss their implications. Finally, Sections 9 and 10 summarize our conclusions and our plans for future work.

2 THE SURVEY AREAS

The seven areas of the survey presented here are centred at: 0020+2947, 0303+2629, 0731+5427, 0938+3218, 1228+5301, 1535+4305, 1737+4215 [RA ($^{h\,m}$), Dec. ($^\circ\,'$), J2000.0], as indicated in Fig. 1. They are situated away from the Galactic plane and are widely spaced in RA, their positions having been determined by the choice of fields for the observations of the VSA. The RA and Dec. ranges are given in Table 1. The total area amounts to 114.7 deg^2, and within this our source list is complete to ≈10 mJy.

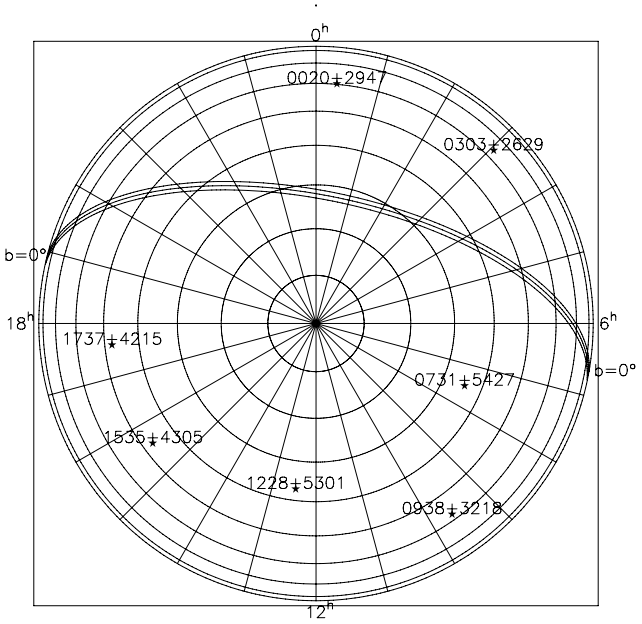

Figure 1. The deeper 9C survey areas: an equatorial plane projection with the North pole at the centre. The declination circles are at intervals of 10° and the Galactic plane is shown.

Table 1. The areas complete to ≈10 mJy.

Field	RA ($^{h\,m\,s}$) to RA ($^{h\,m\,s}$)	Dec. ($^\circ\,'\,''$) to Dec. ($^\circ\,'\,''$)
0020+2947	00 06 48.2 00 33 04.6	+26 37 55 +32 55 20
0303+2629	02 49 36.5 03 16 03.3	+24 26 19 +28 32 04
0731+5427	07 22 05.0 07 40 01.2	+53 09 29 +55 44 20
0938+3218	09 29 38.0 09 46 08.0	+30 43 45 +33 51 55
1228+5301	12 17 08.5 12 38 43.9	+51 27 16 +54 33 45
1535+4305	15 22 16.7 15 47 10.1	+40 43 16 +45 25 52
1737+4215	17 29 40.3 17 43 57.2	+41 13 24 +43 17 30

In each field there are also some much more sensitive areas; this was partly because deeper surveying was required near the centre of the VSA primary beam and partly because on some days there were particularly favourable observing conditions. For the purpose of this paper, in order to assemble a complete sample of a useful size, we have selected a number of subareas with ≈5.5 mJy completeness (as explained in Sections 3 and 4) and these form a total area of 29.1 deg^2 (Fig. 2). They are of various shapes and sizes, so in Table 2 we have described them in terms of small constituent areas bounded by specific RA and Dec. ranges. Although our completeness limit in these regions is ≈5.5 mJy, we have detected many fainter sources, the faintest being only 1 mJy.

3 OBSERVATIONS AND DATA ANALYSIS

3.1 Basic strategy

Since the area within the full width at half-maximum of the RT primary beam is only 0.01 deg^2 and the area to be covered was more than 100 deg^2, we have continued with a rastering technique similar to that described in Paper I, in order to cover the required regions on any reasonable time-scale. As before, the raster maps were used simply to identify peaks corresponding to possible radio sources. Each candidate source was subsequently followed up with a short pointed observation, either to establish a reliable flux density

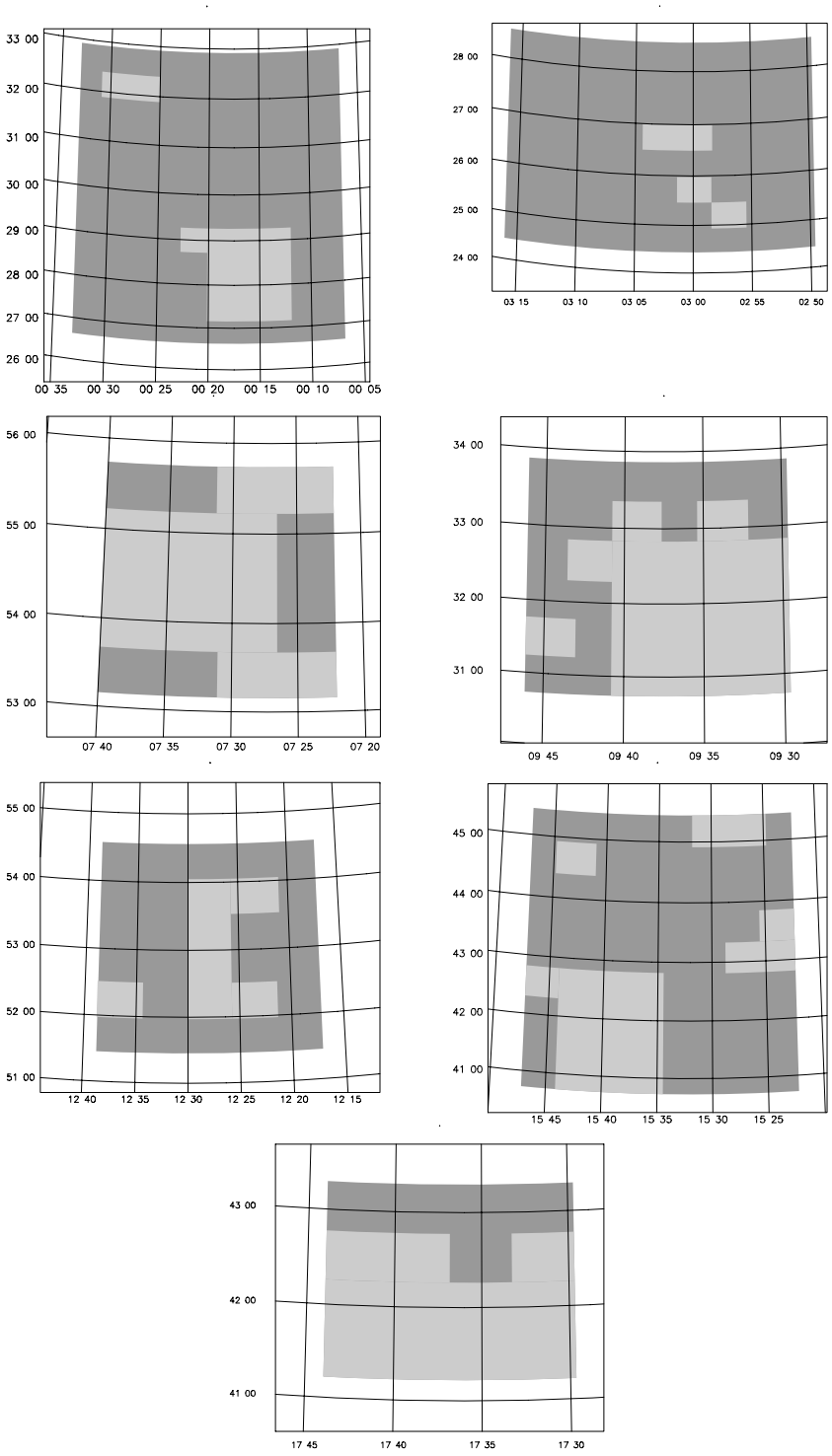

Figure 2. The seven fields, centred at 0020+2947, 0303+2629, 0731+5427, 0938+3218, 1228+5301, 1535+4305 and 1737+4215. The total areas are complete to ≈10 mJy and the deeper areas (shown in paler grey) to ≈5.5 mJy.

or to eliminate it as a false detection. Thereafter, the pointed flux densities were those used for the catalogue, the source counts and the spectral index distributions.

3.2 Raster mapping

We used the RT's East–West array of five aerials to give a resolution of 25×25 cosec δ arcsec^2 and constructed so-called 'raster' maps, each one being generated from a set of observations in a hexagonal pattern of pointing directions. In all, we made 370 raster maps, each of ∼0.34 deg^2, corresponding to some 900 12-h observing runs. Our rastering technique has been described in detail in Paper I, so here we simply give an outline, concentrating on the differences from our earlier method.

A typical raster map was derived from 72 pointing centres in a 9×8 hexagonal array, spaced at intervals of 5 arcmin, as illustrated

Table 2. The areas complete to ≈5.5 mJy.

Field	RA ($^{h\ m\ s}$) to RA ($^{h\ m\ s}$)		Dec. ($^{\circ\ \prime\ \prime\prime}$) to Dec. ($^{\circ\ \prime\ \prime\prime}$)	
0020+2947	00 11 55.7	00 20 08.0	+27 09 39.0	+29 16 04
	00 20 08.0	00 22 45.5	+28 43 43.0	+29 16 04
	00 25 00.8	00 30 54.6	+31 53 24.0	+32 24 07
0303+2629	02 55 27.2	02 58 26.5	+24 56 03.0	+25 27 56
	02 58 26.5	03 01 23.7	+25 27 56.0	+25 58 27
	02 58 21.7	03 04 22.8	+26 29 55.0	+26 59 31
0731+5427	07 22 05.0	07 31 04.6	+53 09 29.0	+53 40 27
	07 26 33.2	07 40 01.2	+53 40 27.0	+55 13 28
	07 22 05.0	07 31 17.7	+55 13 28.0	+55 44 20
0938+3218	09 29 38.0	09 40 46.9	+30 43 45.0	+32 49 53
	09 43 01.8	09 46 08.0	+31 14 44.0	+31 46 05
	09 40 46.9	09 43 35.0	+32 17 15.0	+32 49 55
	09 32 08.6	09 35 23.3	+32 49 53.0	+33 21 31
	09 37 38.7	09 40 46.9	+32 49 53.0	+33 21 16
1228+5301	12 21 19.2	12 25 44.9	+51 58 14.0	+52 30 36
	12 25 44.9	12 30 01.0	+51 58 14.0	+54 02 56
	12 34 22.2	12 38 48.0	+51 58 21.0	+52 30 43
	12 20 54.5	12 25 44.9	+53 31 51.0	+54 02 56
1535+4305	15 34 28.4	15 44 07.5	+40 43 16.0	+42 49 11
	15 44 07.5	15 47 10.1	+42 18 13.0	+42 49 11
	15 22 16.7	15 28 44.7	+42 48 44.0	+43 19 48
	15 22 16.7	15 25 32.3	+43 19 48.0	+43 51 07
	15 40 59.3	15 44 46.9	+44 23 59.0	+44 55 40
	15 24 45.0	15 31 50.2	+44 54 51.0	+45 25 52
1737+4215	17 29 40.3	17 43 57.2	+41 13 24.0	+42 15 51
	17 29 40.3	17 33 16.0	+42 15 51.0	+42 46 40
	17 36 50.1	17 43 57.2	+42 15 51.0	+42 46 40

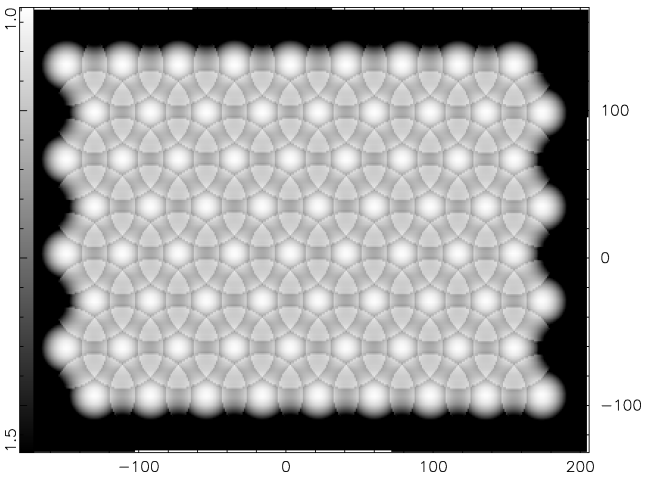

Figure 3. A typical sensitivity map corresponding to a 9 × 8 hexagonal array of pointing directions. White indicates high sensitivity. The coordinates are in map pixels, where 1 pixel represents 8 × 8 arcsec^2.

in Fig. 3. The spacing determined the variation in sensitivity across the map, and 5 arcmin was chosen as an acceptable compromise with observing time. There were six scans through such an array during a 12-h observation, with a dwell time on each centre at each pass of 12 of the 8-s data samples, and a switch to a phase calibrator at intervals during the run. We made 72 small maps (so-called 'component' maps), one for each pointing; at this stage, there was no correction for the primary beam envelope. The *uv* aperture coverage was sparse and was different for each map, as was the effective noise, since each pointing had independent data.

In an improvement on our previous method, we then applied CLEAN to each of the component maps. Since the synthesized beam necessarily varies from map to map, it was not appropriate to apply a joint deconvolution, as can be done in traditional 'mosaicing'. In fact, our technique differs from mosaicing in that, rather than trying to image extended objects that span several primary beam areas, we are only concerned to identify point sources. We therefore calculated an appropriately weighted combination of the CLEANed maps, treating them as independent data and taking the primary beam into account.

The map value M_r at any point on the raster map was derived from the individual map values (m_i) and primary beam values (p_i) of up to three overlapping component maps. We added the map values corrected for the primary beam, (m_i/p_i), weighted by p_i^2. This gave

$$M_r = \left(\sum_{i=1}^{i_{max}} m_i\, p_i\right)\left(\sum_{i=1}^{i_{max}} p_i^2\right)^{-1}, \qquad \text{where} \quad i_{max} = 1, 2 \text{ or } 3.$$

Only the region of each component map out as far as 0.3 of the primary beam maximum was used. The resulting variation in sensitivity over the raster map, even if the component maps had similar noise levels, was as much as 20 per cent, as can be seen from Fig. 3.

We made an estimate of the mean noise, σ, over each raster map and continued to integrate data until we had reached our required sensitivity. For the deeper areas, our criterion was $\sigma \leq 1$ mJy and for the remaining areas $\sigma \leq 2$ mJy. In the event, we finally reached an estimated value for the overall mean noise of 0.90 mJy in the deeper areas and of 1.4 mJy in the remaining areas. However, because of our observing strategy, these noise distributions are not necessarily Gaussian.

3.3 Source extraction

As explained above, the raster maps were used simply to identify peaks corresponding to possible sources, which were subsequently followed up with pointed observations. We first scanned the maps for local maximum pixels $\geq 3\sigma$ and then for each maximum, by interpolation, calculated a corresponding peak value and position. In a change from our earlier method, we now selected peaks $\geq 4.5\sigma$, rather than $\geq 5\sigma$, to form a list of source candidates. This enabled us to find as many of the weaker sources as possible but meant that some 28 per cent of the peaks were rejected as spurious by the follow-up observations. In general, the follow-up was made within a few weeks of the raster scan and was simply a short pointed observation of 10–15 min with a resolution of 25 × 25 cosec δ arcsec^2. The final source lists were compiled from the pointed flux densities. The errors in these are dominated by a random uncertainty in the flux calibration of ∼5 per cent.

4 COMPLETENESS

Although we can be sure that every source in our catalogue is genuine, since each raster peak was followed up with a pointed observation, assessment of the completeness limits of our source lists is not straightforward. This is because the original candidate sources were found from raster maps with a range of noise levels. As well as the difference in noise from raster map to raster map, there is also variation in noise on small spatial scales within each map, arising from the rastering technique. We cannot assume that

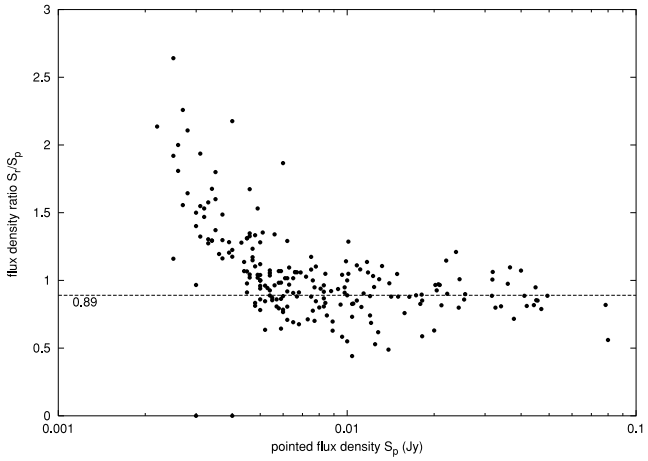

Figure 4. Plot of the ratio (S_r/S_p) of the raster peak flux density to the pointed flux density versus S_p, for the deeper areas. (Where the ratio is shown as zero, the corresponding source lies in an area of a raster map which is hard to interpret. A pointed observation has been made, but there is no definitive raster flux density.)

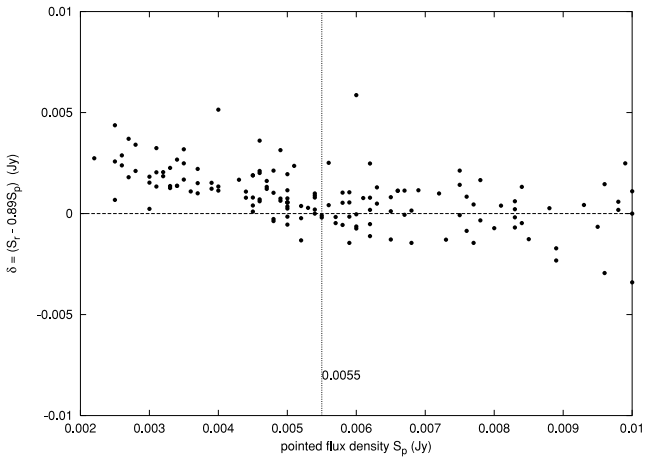

Figure 5. Plot of δ versus S_p for the deeper areas, where $\delta = S_r - 0.89S_p$.

Table 3. Statistics of δ values.

Range of S_p (mJy)	Total number of sources	No. with $\delta > 0$	No. with $\delta < 0$
$5.5 \leq S_p < 6.5$	25	13	12
$5.0 \leq S_p < 6.0$	33	21	12
$4.5 \leq S_p < 5.5$	40	33	7
$5.5 \leq S_p < 10.0$	65	36	29

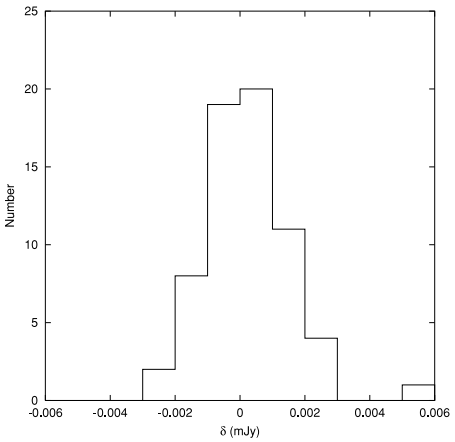

Figure 6. Histogram of the δ values for the 65 sources in the range 5.5 mJy $\leq S_p < 10$ mJy in the deeper areas.

the noise is Gaussian, even over small areas, so we have adopted the following somewhat unconventional approach to the problem.

Taking the deeper areas (Table 2) first, we have plotted the ratio, (S_r/S_p), of the raster peak to the pointed flux density versus S_p, as in Fig. 4. We find that, for the brighter sources, in the range $\geq$10 mJy where we can assume completeness, there is a scatter about a median ratio of 0.89. This offset of $\sim$10 per cent in the median value is attributed to the problem of allowing sufficient telescope settling time during the raster scans; there was a necessary compromise between keeping as many of the observed data samples as possible and discarding those with excessive pointing errors. For the weaker sources, the ratio rises progressively with decreasing flux density because at these levels the peaks detected on the raster maps are preferentially those boosted by a positive local noise contribution. In order to estimate the completeness limit, we have investigated at what level, with decreasing pointed flux density, S_p, we start to lose a significant number of sources.

We can regard the flux density from a pointed observation, S_p, as the 'true' value, since we know it represents a real source and it has an uncertainty of only 5 per cent, i.e. a signal-to-noise ratio value of 20. However, the corresponding peak S_r that appears on the raster map will include an added contribution, δ, arising from the local noise. Allowing for the scalefactor of 0.89 mentioned above, we can express the response on a raster map, S_r, from a source of flux density, S_p, as $S_r = (0.89 \times S_p) + \delta$, where δ can be positive or negative.

In Fig. 5, we have plotted δ (i.e. $S_r - 0.89S_p$) versus S_p, in the range $S_p < 10$ mJy, to illustrate the scatter about the line $\delta = 0$. For sources above the completeness limit, we expect approximately equal numbers with positive and negative values of δ, whereas at decreasing flux density levels there will be an increasing bias towards detecting sources with positive, rather than negative, δ values. We have investigated at what value of S_p this bias becomes significant.

We see from Fig. 5 that there appears to be a significant increase in the proportion of sources with $\delta_\sigma > 0$ in the range 4.5 mJy $< S_p < 6.5$ mJy, so we have examined this region in more detail. Our results are presented in Table 3. These are small numbers, but they do indicate a steep change in the statistics below 5.5 mJy. Taking 5.5 mJy as the lower limit, we find that, for the 65 sources in the range 5.5 mJy $\leq S_p < 10$ mJy, there are 36 with $\delta > 0$ and 29 with $\delta < 0$. In view of the Poisson errors, we consider this difference not to be significant. Also, the histogram of these delta values, shown in Fig. 6, is approximately symmetrical about $\delta = 0$, apart from one outlier.

It is difficult to put a precise figure on the percentage completeness at 5.5 mJy but, given the statistics, we conclude it is at least 90 per cent. There are 135 sources above this level and 81 below. The advantage of our method is that it deals both with the problem of the varying noise levels over the raster maps and with the effect of any source variability between the raster and pointed measurements, which together can produce the wide scatter in the values of δ.

For the total areas (Table 1), we have applied similar tests on (S_r/S_p) and δ, using the higher flux densities, and conclude we have a completeness limit of approximately 10 mJy, giving us 307

Table 4. A section from the source catalogue. The letter 'D' means that the source lies in one of the deeper areas listed in Table 2. In the comment, column 'b' denotes a binary source and 'e' an extended source. The full table is available with the online version of this paper (see Supporting Information).

Source name		RA J2000 (h m s)	Dec. J2000 (° ′ ″)	Flux density (Jy)	Date (yymmdd)	Comment
9CJ0015+3123		00:15:47.5	31:23:35	0.0127	020505	e
9CJ0015+2718	D	00:15:58.0	27:18:54	0.0031	031124	
9CJ0016+2804	D	00:16:02.4	28:04:28	0.0027	031124	
9CJ0016+3158		00:16:07.4	31:58:53	0.0092	041016	
9CJ0016+3239		00:16:11.0	32:39:26	0.0230	041228	
9CJ0016+2945		00:16:13.0	29:45:11	0.0156	010815	
9CJ0016+3238		00:16:13.6	32:38:37	0.0264	041228	
9CJ0016+3139		00:16:40.6	31:39:04	0.0110	030203	b
9CJ0017+3209		00:17:02.2	32:09:19	0.0345	041016	
9CJ0017+2733	D	00:17:04.6	27:33:43	0.0062	031124	

sources above the limit and 336 below. We should also explain that within the areas presented in this paper, there is a shortfall in the number of sources above 100 mJy as compared with the number expected from the source count in Paper I (see Section 6). This is because these VSA fields were deliberately selected from our earlier 9C fields to contain as few sources above 100 mJy as possible.

5 THE SOURCE CATALOGUE

A short section of the catalogue is shown in Table 4. The whole list is available online at http://www.mrao.cam.ac.uk/surveys together with the relevant tables, i.e. Tables 1 and 2 from this paper. We have included all 643 sources, which means that a large number of them are below our completeness limits of ≈10 mJy for the total areas and ≈5.5 mJy for the deeper areas, the faintest being only 1 mJy. Sources which lie within the deeper areas are marked D in the catalogue. Where there are two apparently independent sources with the same abbreviated source name, we have added a or b to the name. An obvious binary source is listed as one source, with a centroid position and integrated flux density, and is denoted by 'b' in the comment column. An 'e' in the comment column means that, in the pointed observation, the source appears extended relative to the synthesized beam size.

We have not assigned individual error estimates to the source parameters. The position of a source is derived from a raster map, unless the follow-up pointed observation indicates a position differing by more than 10 arcsec, in which case that is substituted. However, since there are large overlaps between adjacent raster maps and a number of sources appear on more than one map, it has been possible to make a general estimate of the position accuracy. Taking the 0020+2947 field, we find 39 sources with repeat position measurements. Apart from one extended source, in no case do the measurements differ by more than 10 arcsec and the median difference is ∼4 arcsec. The flux densities are in the range 4.6 to 68.3 mJy. For the brighter sources we can refer to Paper I, where we matched a sample of 17 sources, all >60 mJy at 15.2 GHz, with their counterparts in the Jodrell Very Large Array (VLA) calibrator survey (Wilkinson et al. 1998, and references therein), finding an accuracy for these sources of better than 3 arcsec.

Our flux densities are derived from the pointed observations and the uncertainty in these is dominated by the uncertainty in the flux calibration, which is ∼5 per cent. In the case of an extended source, we record the integrated flux density. Since a number of the sources are highly variable, the dates of the pointed observations are also included in the catalogue.

In addition to the catalogues presented in this paper and in Paper I, there are source lists from further areas of the 9C survey yet to be published, some complete to 25 mJy and some to 10 mJy. We plan to make these available online in due course. However, none of the unpublished areas is deeper than those reported here.

6 SOURCE COUNTS

We have calculated the source counts from the pointed flux densities, using the values in our final catalogue. The count for the sources in the total areas is shown in Fig. 7 which indicates the lower completeness limit of 10 mJy and also the shortfall above 100 mJy explained in Section 4. Fig. 8 is a similar plot for the subset of these sources which lie in the deeper areas.

With these counts, we are now able to extend the original 9C count to a lower flux density level. We have combined data from Paper I in the range $S \geq 25$ mJy with data from this paper in the range $10 \leq S < 25$ mJy from the total areas and $5.5 \leq S < 10$ mJy

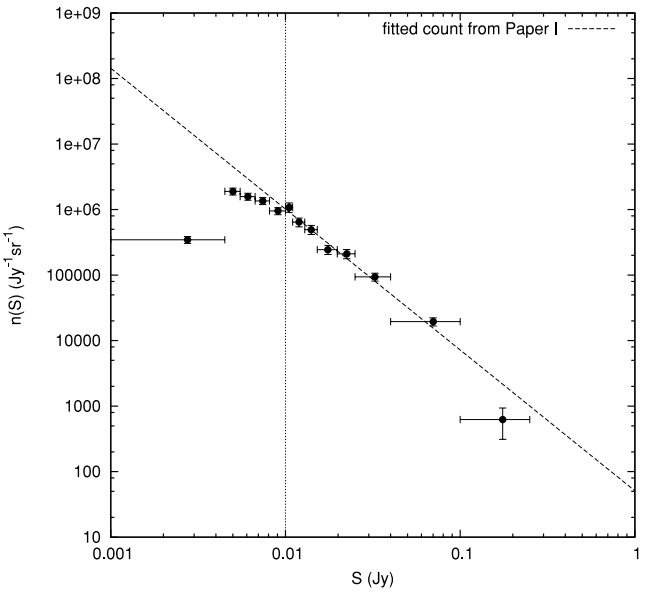

Figure 7. The source count for the sources in the total areas, showing the lower completeness limit of ≈10mJy and the shortfall above 100 mJy.

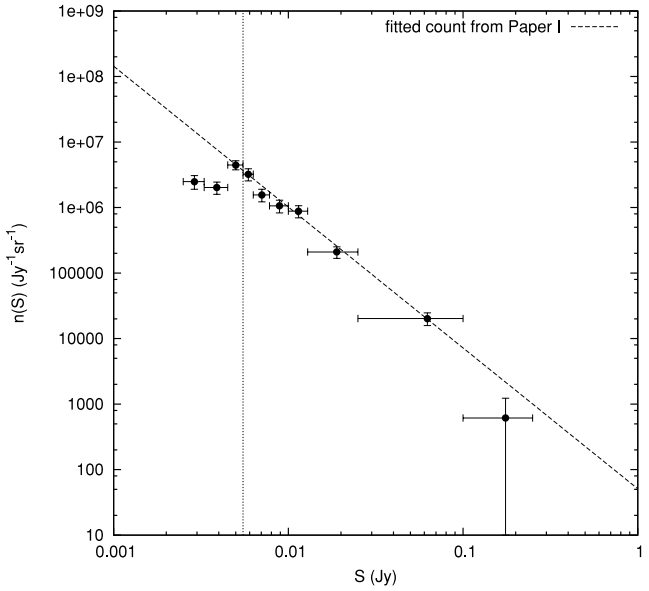

Figure 8. The source count for the sources in the deeper areas, showing the lower completeness limit of ≈5.5mJy and the shortfall above 100 mJy.

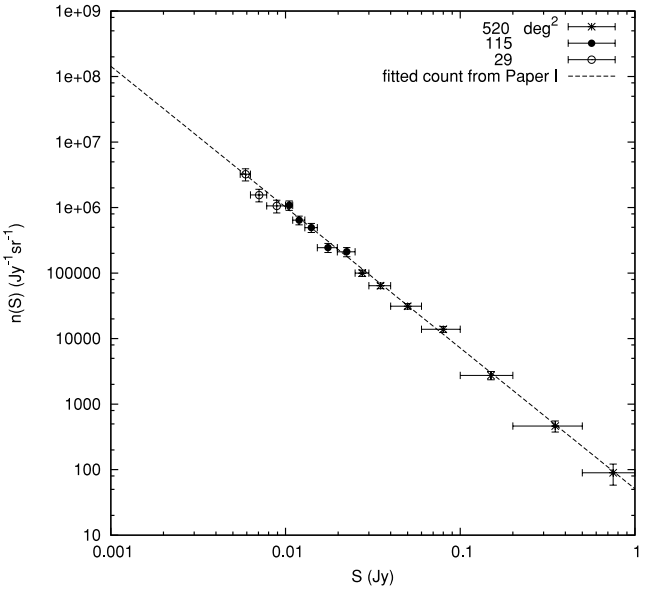

Figure 9. Differential count extended to 5.5 mJy.

Table 5. The data used in the combined count.

Bin start *S*/Jy	Bin end *S*/Jy	Number *N*	Area (sr)
0.0055	0.00 63	23	0.008 856
0.0063	0.0078	21	0.008 856
0.0078	0.0100	21	0.008 856
0.0100	0.0110	38	0.034 939
0.0110	0.0129	43	0.034 939
0.0129	0.0152	40	0.034 939
0.0152	0.0198	40	0.034 939
0.0198	0.0250	39	0.034 939
0.025	0.030	80	0.158 41
0.030	0.040	104	0.158 41
0.040	0.060	103	0.158 41
0.060	0.100	94	0.158 41
0.100	0.200	49	0.158 41
0.200	0.500	27	0.158 41
0.500	1.000	8	0.158 41

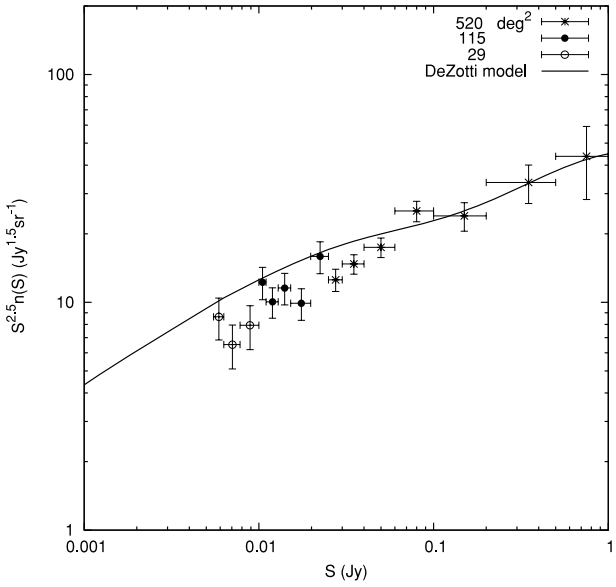

Figure 10. Normalized count compared with the de Zotti model.

from the deeper areas (see Table 5). In view of the discussion in Section 4, and considering the Poisson errors on N, we have not attempted to make any correction for incompleteness. In fact, we find that in the lowest bin of the combined count there are 11 sources with $\delta > 0$ and 12 with $\delta < 0$. (See Section 4 for the definition of δ.) Also, as explained in Paper I, the effect of the random errors of ∼5 per cent in the pointed flux densities is negligible compared with the Poisson errors on N, amounting to an increase of <1 per cent in N in each bin. We have, however, applied a correction for the bin width (W) in the same way as before. If S_c is the value of S at the centre of a bin, the corresponding N is multiplied by a factor of $(1 - r^2)$ where $r = W/2S_c$.

At the completeness limit of 5.5 mJy, the survey continues to be limited by noise rather than confusion; we estimate that above this level there are typically 2000 synthesized beam areas per source.

Fig. 9 shows the differential count $n(S)$ and we see that, down to 5.5 mJy, there is no evidence for any significant change from the fitted count $n(S)$ calculated in Paper I, i.e.

$$n(S) \equiv \frac{\mathrm{d}N}{\mathrm{d}S} \approx 51 \left(\frac{S}{\mathrm{Jy}}\right)^{-2.15} \mathrm{Jy}^{-1}\,\mathrm{sr}^{-1}.$$

In Fig. 10, we compare our normalized count $S^{2.5}n(S)$ with that derived from the model of de Zotti et al. (2005) and note that our count appears to lie somewhat below their prediction in the lower flux density range.

These two figures effectively update the plots in figs 6 and 7 of Paper I. We should mention here that we found retrospectively that the positions of two points in each of those figures are in error. These are the two open circles corresponding to the higher flux bins of the deeper survey. In fact, since they lie in the flux density range of the main survey, they do not affect any of the arguments or conclusions in that paper and can simply be ignored.

7 CORRELATION WITH NVSS – RESULTS

In this section, we present the results of our investigations but defer any discussion of their implications to Section 8.

7.1 Matching the catalogues

We have attempted to match the 643 sources in our catalogue with the catalogue from the NVSS 1.4-GHz survey, which has a resolution of 45 arcsec (not dissimilar to our own) and a completeness of 50 per cent at ≈2.5 mJy rising rapidly to 99 per cent at 3.4 mJy. In the first instance, we searched for a counterpart within 40 arcsec of each of the 9C sources and then in every case inspected the corresponding NVSS contour plot, paying particular attention to sources which had multiple matches within 40 arcsec and to those where there was no match within 20 arcsec. For about 90 per cent of the sources, the matching was straightforward; the remainder, however, required further attention in order to make the appropriate correlation of flux densities. For example, some binary sources had a single entry in the 9C catalogue but appeared separately in the NVSS catalogue and, conversely, there were some single NVSS sources which appeared as separate components in 9C. Where possible, we made use of the deeper Faint Images of the Radio Sky at Twenty cm (FIRST) 1.4-GHz survey (Becker, White & Helfand 1995), with its resolution of 5 arcsec, to assist in resolving ambiguities.

Our correlation is illustrated in Fig. 11. In all, out of the 643 sources in our list, there were 21 with no counterpart in the NVSS catalogue, though two of these did appear in FIRST. Also, a number of them were found to be coincident with one or two contours on the NVSS plots but clearly these were not significant enough detections to justify their inclusion as sources in the NVSS catalogue.

7.2 9C sources not in the NVSS catalogue

Table 6 lists the 21 sources in our total source list which do not appear in the NVSS catalogue. Only one of these lies in the deeper areas (see the dotted box in the top plot of Fig. 13) and the others are all in the total areas. By dividing these 21 sources into three flux density bins, as shown in Table 7, we can gain an indication of the proportion of 9C sources, with no counterparts in NVSS, as a function of flux density. We are complete only in the highest bin ($10 \leq S < 15$ mJy), for which we find 4.3 per cent of sources with no NVSS counterpart. Assuming that the proportion of sources with no counterpart increases with decreasing flux density, our estimates of the proportions of 'missing' sources are likely to be underestimates for the two lower flux density bins. This is because these bins are incomplete; sources with higher fluxes are preferentially detected in these incomplete bins, yet it is the brighter sources that are more likely to have an NVSS counterpart.

We should note that several of the sources have been observed at other frequencies. For example, several are close to sources in the Two-Micron All-Sky Survey (Skrutskie et al. 2006) and *ROSAT* all-sky survey (Voges et al. 1999) catalogues. However, here we are concerned with the number of sources at 15 GHz that would be missed by reliance on the NVSS catalogue.

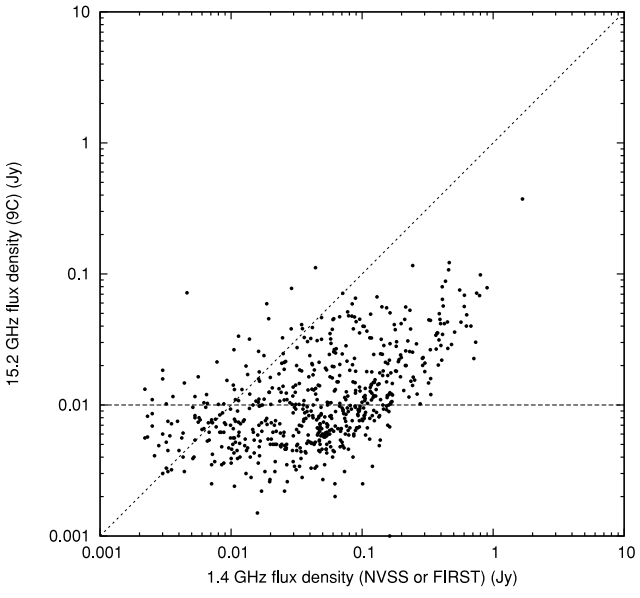

Figure 11. Plot of RT 15.2-GHz pointed flux densities versus NVSS (or FIRST) 1.4-GHz flux densities, with a line indicating zero spectral index. The horizontal line is the estimated completeness limit.

Table 6. 9C sources without corresponding matches in NVSS. Flux densities for those sources appearing in the FIRST survey are provided, along with the spectral index based upon the FIRST flux density. For sources not appearing in FIRST, an upper limit to the spectral index is provided by assuming a flux density of 3.4 mJy (the estimated 99 per cent completeness limit of NVSS) at 1.4 GHz.

RA (J2000)	Dec. (J2000)	15.2-GHz flux density (mJy)	1.4-GHz flux density (mJy)	α
17:40:17.1	+42:14:31	14.0		−0.59
02:53:29.4	+27:57:45	13.0		−0.56
00:27:28.0	+28:08:10	10.9		−0.49
00:14:19.0	+31:33:45	10.2		−0.46
15:37:42.1	+43:49:12	10.2	0.87	−1.03
12:35:22.9	+53:11:29	6.2		−0.25
00:11:51.7	+27:57:19	6.0		−0.24
09:44:27.2	+33:03:22	6.0		−0.24
09:37:22.6	+32:01:04	5.3		−0.19
09:34:35.9	+30:44:05	5.0		−0.16
09:30:36.0	+30:48:54	4.5		−0.12
17:33:11.1	+41:21:05	4.5		−0.12
00:27:10.3	+26:55:42	4.4		−0.11
15:32:04.6	+42:51:52	4.1	2.56	−0.20
03:14:20.8	+26:26:27	4.0		−0.07
15:38:47.8	+43:51:18	3.5		−0.01
17:42:52.2	+43:09:51	3.2		0.03
00:15:58.0	+27:18:54	3.1		0.04
00:31:12.7	+27:12:58	3.0		0.05
07:27:18.0	+55:10:45	3.0		0.05
15:40:52.8	+44:16:22	2.6		0.11

Table 7. 9C sources with no NVSS counterpart as a function of flux density.

Flux density range (mJy)	Number of 9C sources	Number of sources with no NVSS counterpart
$S < 4.2$	62	8 (12.9 per cent)
$4.2 \leq S < 10$	281	8 (2.8 per cent)
$10 \leq S < 15$	117	5 (4.3 per cent)

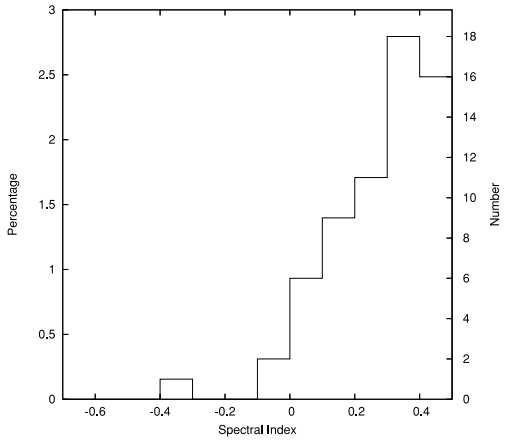

Figure 12. Histogram of the spectral index distribution $\alpha_{1.4}^{15.2}$ for a sample selected from NVSS with $S_{1.4} \geq 32.95$ mJy, showing the percentage of sources with flat and rising spectra. $S \propto \nu^{-\alpha}$.

7.3 Samples selected from NVSS at 1.4 GHz

It is not possible to calculate a full spectral index distribution for a sample of NVSS sources complete to a level of 3.4 mJy, since many of the steep spectrum sources will not be detectable in our survey. We can, however, investigate the proportion of flat and rising spectrum sources in the NVSS catalogue for different cut-offs in 1.4 GHz flux density, where we use 'flat and rising' to refer to sources with $\alpha_{1.4}^{15.2} \leq 0.5$. (We define α by $S \propto \nu^{-\alpha}$.)

We have selected all sources from the NVSS catalogue, lying in the areas complete to 10 mJy at 15.2 GHz, with $S_{1.4} \geq 32.95$ mJy; in total, 644 sources are selected. These selection criteria ensure that any sources with $\alpha_{1.4}^{15.2} \leq 0.5$ will have $S_{15.2} \geq 10$ mJy, our completeness limit at 15.2 GHz. Of the 644 sources selected, 63 are found to have $\alpha_{1.4}^{15.2} \leq 0.5$. In other words, we find that 9.8 per cent of sources with $S_{1.4} \geq 32.95$ mJy have $\alpha_{1.4}^{15.2} \leq 0.5$. We have plotted this flat and rising part of the spectral index distribution $\alpha_{1.4}^{15.2}$ at 1.4 GHz as a histogram in Fig. 12. We have also taken a lower flux density cut at 1.4 GHz of 10 mJy (again in our total areas), which enables us to investigate sources with $\alpha_{1.4}^{15.2} \leq 0$ for a somewhat deeper sample.

Similarly, we have taken appropriate NVSS flux density cuts in the deeper areas, complete to 5.5 mJy at 15.2 GHz, to enable us to investigate the rising, and flat and rising side of the distribution at lower flux densities. Our results are summarized in Table 8.

7.4 Samples selected at 15.2 GHz

At 15 GHz it has been possible to take complete flux-limited samples and investigate both spectral index distributions and spectrally selected source counts.

7.4.1 Spectral index distributions

A histogram of the spectral index distribution $\alpha_{1.4}^{15.2}$ for the 111 sources with $5.5 \leq S < 25$ mJy and lying in our deep areas is shown in Fig. 13. (We define α by $S \propto \nu^{-\alpha}$.) The figure also shows the spectral index distributions, over the same range of frequencies, for sources with $25 \leq S < 100$ mJy and $S \geq 100$ mJy; these distributions contain 381 and 84 sources, respectively, and were originally included in Paper I. They are derived from an area of 520 deg^2 complete to $\approx$25 mJy. In Table 9, we have summarized some important features of the distributions; it is clear from this table and Fig. 13 that, as one moves to lower flux densities, the proportion of sources with flat and rising spectra decreases.

In order to assess the significance of the shift in median spectral index with flux density, we have combined the spectral indices of the 576 sources to form a single spectral index distribution, which we have plotted as a histogram in Fig. 14. We assume that there is an underlying spectral index distribution which has no dependence on flux density and that the combined data represent our best approximation to this distribution. For each of our flux density bins, we calculate the probability of drawing the observed number of sources from the combined distribution and finding a median spectral index as extreme as those observed, using a Monte Carlo simulation of 10^6 realizations. For example, for the lowest flux density bin, for each realization, we draw, at random, 111 values from the combined spectral index distribution and find the median spectral index. We find 14 realizations, out of 10^6, in which this value is greater than or equal to the observed value of 0.79 and conclude that the probability of drawing 111 sources from the combined distribution and observing a median as or more extreme than 0.79 is 2.8×10^{-5}.

Table 10 provides a summary of the results from the simulations. It shows that the median spectral index observed for the middle flux density bin is not significantly different from that of the combined distribution of Fig. 14. However, the probabilities of having obtained median spectral indices more extreme than observed, for the two outer flux density bins, by drawing sources randomly from the combined distribution are very small. Consequently, we can reject our null hypothesis that the underlying spectral index distribution has no dependence on flux density, with a high level of confidence. In other words, the shift in the median spectral index with flux density is significant.

7.4.2 Source counts for samples with $\alpha_{1.4}^{15.2} \leq 0.5$ and $\alpha_{1.4}^{15.2} > 0.5$

To shed further light on the shift in spectral index distribution with flux density, we have investigated the source counts for samples with $\alpha_{1.4}^{15.2} \leq 0.5$ and $\alpha_{1.4}^{15.2} > 0.5$. For this investigation, we have used the same sources as in the analysis in Section 7.4.1: in other words, the sources with $5.5 \leq S < 25$ mJy from our deepest

Table 8. Proportions of rising, and flat and rising sources in the NVSS catalogue. Samples selected at 1.4 GHz.

Flux density cut at 1.4 GHz (mJy)	Number of NVSS sources	9C area	Select sources with	Number of sources selected
32.95	644	110 deg^2 complete to 10 mJy	$\alpha_{1.4}^{15.2} \leq 0.5$	63 (9.8 per cent)
10.0	1891	110 deg^2 complete to 10 mJy	$\alpha_{1.4}^{15.2} \leq 0$	20 (1.1 per cent)
18.12	295	29 deg^2 complete to 5.5 mJy	$\alpha_{1.4}^{15.2} \leq 0.5$	27 (9.2 per cent)
5.5	770	29 deg^2 complete to 5.5 mJy	$\alpha_{1.4}^{15.2} \leq 0$	11 (1.4 per cent)

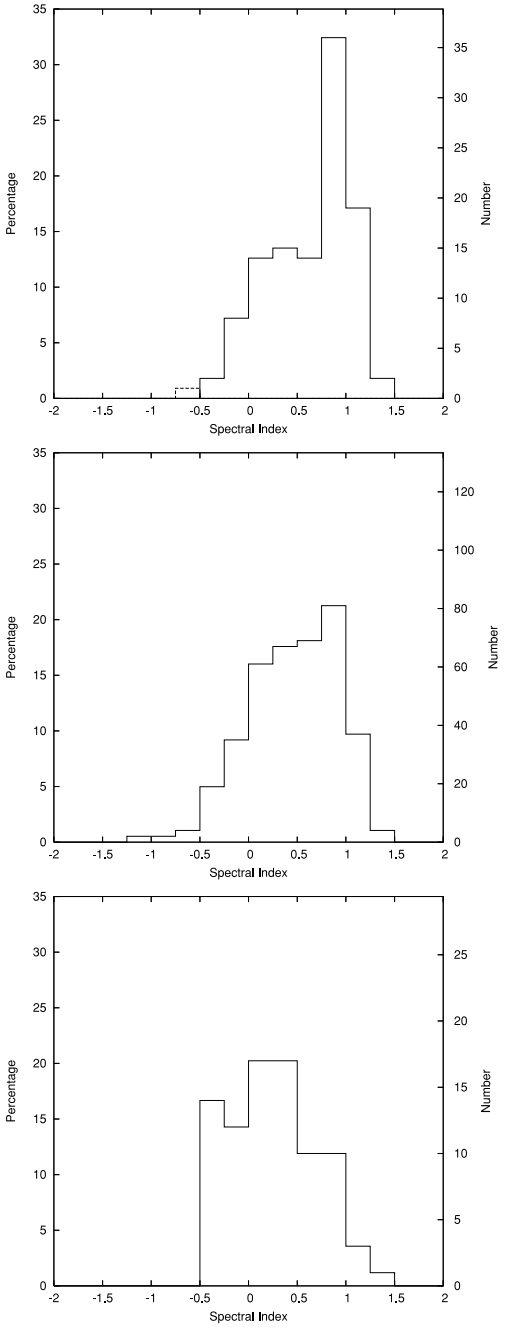

Figure 13. The $\alpha_{1.4}^{15.2}$ spectral index distributions for samples selected at 15.2 GHz in three flux density ranges. From the top: $5.5 \leq S < 25$ mJy, $25 \leq S < 100$ mJy and $S \geq 100$ mJy, with median values of 0.79, 0.51 and 0.23, respectively. We define α by $S \propto \nu^{-\alpha}$ (the dotted box in the top plot indicates a limiting value of α for a source not in NVSS).

areas, complete to 5.5 mJy, and the sources with $S \geq 25$ mJy from the areas presented in Paper I, complete to 25 mJy. Of the 576 sources used for this analysis, 289 have $\alpha_{1.4}^{15.2} \leq 0.5$ and 287 have $\alpha_{1.4}^{15.2} > 0.5$.

We have binned the data for the two samples in flux density, choosing the bins so that there were as far as possible the same number of sources in each, and plotted the differential source count for each of the samples in Fig. 15. In each case, we have fitted a function of the form AS^b to the differential source count, by using a least-squares fit, taking account of the Poisson error on the number

Table 9. Some statistics for the spectral index distributions $\alpha_{1.4}^{15.2}$. Samples selected at 15 GHz.

15.2-GHz flux density range (mJy)	Number of sources	Number of sources with $\alpha_{1.4}^{15.2} \leq 0$	Number of sources with $\alpha_{1.4}^{15.2} \leq 0.5$	$\tilde{\alpha}_{1.4}^{15.2}$
$5.5 \leq S < 25$	111	11 (10 per cent)	40 (36 per cent)	0.79
$25 \leq S < 100$	381	62 (16 per cent)	190 (50 per cent)	0.51
$S \geq 100$	84	26 (31 per cent)	60 (71 per cent)	0.23

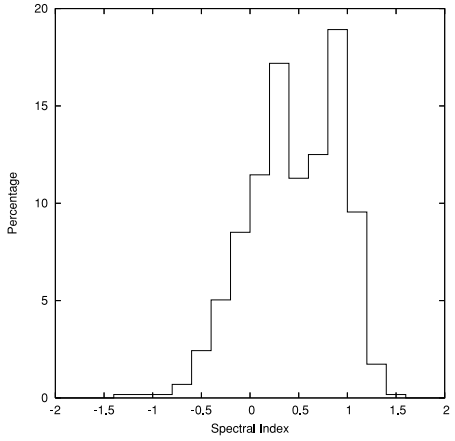

Figure 14. The $\alpha_{1.4}^{15.2}$ spectral index distributions in Fig. 13 combined into one distribution. $S \propto \nu^{-\alpha}$.

of sources in each bin and the width of the bins. The fitted counts are shown, along with the data, in Fig. 15. For the sample with $\alpha_{1.4}^{15.2} \leq 0.5$, we find $b \sim -1.90$ and for the sample with $\alpha_{1.4}^{15.2} > 0.5$, $b \sim -2.27$. There are equal numbers of sources with $\alpha_{1.4}^{15.2} \leq 0.5$ and $\alpha_{1.4}^{15.2} > 0.5$ at $S \sim 44$ mJy.

We can see from the error bars in Fig. 15 that the fitted counts for the two samples differ significantly and that the total 9C count is dominated by sources with flat and rising spectra at the bright end, but by sources with steeply falling spectra at the fainter end. This is consistent with our observed variation of spectral index distribution with flux density.

8 CORRELATION WITH NVSS – DISCUSSION

The purpose of our correlation with NVSS has been to explore the spectral characteristics of the source population at 15 GHz. We have been able to investigate the properties of flux-limited samples selected at both 1.4 and 15 GHz. This cannot tell us anything about the shape of the individual source spectra between the two frequencies (for example, which sources have a peak in this range), but it enables us to compare the two populations. In particular, it can provide a useful test on the reliability of using a low-frequency survey as a basis for predicting the nature of the source population at much higher frequencies.

8.1 Variability

The measurements are not, of course, simultaneous, so we need to consider the effect of variability. In a 3-yr study of the variability of a sample of 48 9C sources at 15 GHz, Bolton et al. (2006a) found 29 per cent to be variable above the calibration uncertainty of ∼6 per cent and, of these, 8 per cent to be variable above a

Table 10. Results from a Monte Carlo simulation, of one million realizations, to assess the significance of the shift in median spectral index with flux density.

15-GHz flux density range (mJy)	Number of simulated sources	Min. $\tilde{\alpha}_{1.4}^{15.2}$	Max. $\tilde{\alpha}_{1.4}^{15.2}$	Mean $\tilde{\alpha}_{1.4}^{15.2}$	Number of realizations with $\tilde{\alpha}_{1.4}^{15.2}$	Probability of drawing median more extreme than observed
$5.5 \leq S < 25$	111	0.166	0.817	0.477	>0.79 is 14	2.8×10^{-5}
$25 \leq S < 100$	381	0.311	0.685	0.474	>0.51 is 212833	0.426
$S \geq 100$	84	0.081	0.879	0.478	<0.23 is 161	3.2×10^{-4}

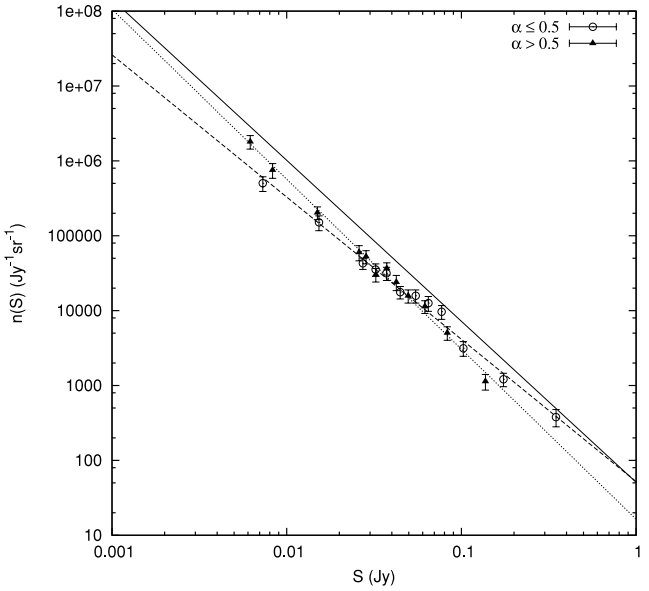

Figure 15. Source counts for samples selected at 15.2 GHz, with $\alpha_{1.4}^{15.2} \leq 0.5$ (dashed line) and $\alpha_{1.4}^{15.2} > 0.5$ (dotted line). The solid line shows the total 9C count.

20 per cent level. Observations at lower frequencies indicate much lower levels of variability. Riley & Green (1998), in a 1-yr study at 1.4 GHz, found fewer than 1 per cent of the sources to have varied by more than 20 per cent. Kellermann & Pauliny-Toth (1968) have shown that even sources with high variability at 2-cm wavelength exhibit little variability at 20 cm. We therefore assume that if there is any bias in our spectral index distributions, it would arise primarily from variability at 15 GHz rather than at 1.4 GHz.

In general, in selecting samples, variability can produce a bias wherever flux density cuts are made on the data, as when the data are divided into bins. We first consider samples selected from NVSS. For these, the low variability at 1.4 GHz will have a negligible effect on the actual sample selection. Also, within the sample, since the variability at 15 GHz can be either up or down and is uncorrelated between sources, there will be no systematic bias.

However, for samples selected at 15 GHz, there will be a possible systematic bias in the sample selection. This is because of the shape of the source count. At the lower end of the bin, the number of sources with positive variation that are included with be marginally higher than the number with negative variation that are rejected. The opposite effect will occur at the top end of the bin, but it will not be sufficient to completely offset the bias. This means that in the sample as a whole, there is likely to be a slightly higher proportion of sources in their positive, rather than negative, phase of variation, which in turn would shift the spectral index distribution slightly in the flatter direction. We discuss in Sections 8.4.1 and 8.4.2 how any small bias might affect our results.

8.2 9C sources not in the NVSS catalogue

An important result is the number of sources that we have detected at 15.2 GHz which do not appear in the NVSS catalogue and, in particular, that in the flux density range of 10 to 15 mJy there are as many as 4.3 per cent not in NVSS. We are not suggesting that these are necessarily unusual sources. Several have been observed at other frequencies, two appear in FIRST and none of the limiting spectral indices quoted in Table 7 is particularly extreme. Our concern is with the relevance to work that relies on the NVSS catalogue to identify sources for surveying at high frequency. It means that at low flux densities more than 4 per cent of the sources could be missed. This could lead to errors in the estimates of high-frequency source counts and in the selection of individual sources for projecting out of high-frequency CMB data.

8.3 1.4-GHz samples

As we have seen, it is not possible to calculate a full spectral index distribution for a sample of sources selected from NVSS at 1.4 GHz, but it is useful to explore the flat and rising side of the distribution. Here, we can assume that any effect from variability is insignificant, since the selection is made at the lower frequency of 1.4 GHz rather than at 15 GHz. We find that, for complete samples of sources above 32.95 and 18.12 mJy at 1.4 GHz, there are 9.8 and 9.2 per cent respectively with $\alpha_{1.4}^{15.2} \leq 0.5$, and for complete samples above 10 and 5.5 mJy at 1.4 GHz, there are 1.1 and 1.4 per cent respectively with $\alpha_{1.4}^{15.2} \leq 0$. The differences here, between 9.8 and 9.2 per cent and between 1.1 and 1.4 per cent, are not significant given the size of the samples, but we note that the values are very close to those found by Mason et al. (2009) for their 1.4 to 31 GHz spectral indices.

8.4 15.2-GHz samples

8.4.1 Comparison with 1.4-GHz samples

We see that the proportions of sources with $\alpha_{1.4}^{15.2} \leq 0$ and $\alpha_{1.4}^{15.2} \leq 0.5$ in samples selected at 15.2 GHz (Table 9) are significantly higher than those in samples selected at 1.4 GHz (Table 8). Although there may be a very small bias towards flatter spectra in the 15-GHz samples, arising from variability, this is negligible relative to the size of the effect.

This result, that a higher proportion of flat and rising spectrum sources are selected at the higher frequency than at the lower frequency, has been recognized before (see, for example, Kellermann, Pauliny-Toth & Davis 1968; Peacock & Wall 1981). It arises because a number of the steep spectrum sources which appear in the

lower frequency samples tend to fall below the flux density cut-off at the higher frequency. Kellermann et al. (1968) explain that it is 'a direct result of the finite dispersion in the distribution of spectral indices and of the form of the number–flux relation'. They demonstrate the effect formally in the simplified case where the source count is a simple power law and the spectral index distribution is independent of flux density.

8.4.2 Correlation between spectral index and flux density

We find that for samples selected at 15.2 GHz in three flux density bins, there is a significant decrease in the median $\alpha_{1.4}^{15.2}$ and increase in the proportion of flat and rising sources with increasing flux density. Although, as we have seen, there may be a very small shift towards flatter distributions arising from variability, this will be in the same direction in each bin and so does not affect our conclusion. The same effect is demonstrated by our plot of the separate source counts for sources with $\alpha_{1.4}^{15.2} \leq 0.5$ and $\alpha_{1.4}^{15.2} > 0.5$ (Fig. 15).

We cannot identify any observational bias that might produce this trend in the median $\alpha_{1.4}^{15.2}$ values, but we can compare our results with those of Bolton et al. (2004). They made simultaneous multifrequency observations at 1.4, 4.8, 15.2, 22 and 43 GHz of flux-limited samples of sources selected from 9C at 15.2 GHz and found that raising the flux limit of the 9C sample produced a significant increase in the fraction of rising spectrum sources. Their analysis differed from ours in that each of their samples had only a lower flux density limit and no upper limit and also they classified the sources in terms of their 1.4 to 4.8 GHz rather than their 1.4 to 15.2 GHz spectral indices. However, they also showed that the 1.4 to 4.8 GHz spectral indices from simultaneous measurements were highly correlated with the 1.4 to 15.2 GHz spectral indices obtained by simply matching 9C with NVSS, which is what we have done here. We believe we have observed a significant correlation between spectral index distribution and flux density and that this does appear to be consistent with the work of Bolton et al. (2004).

In order to assess whether such a change in spectral index distribution is physically reasonable over such a relatively small range of flux density, we have constructed the following highly simplified model. We have not attempted to optimize the model in order to fit our data – a full physical model of the sort proposed by de Zotti et al. (2005) contains a number of different source populations and uses much more sophisticated parametrization. Our aim here is simply to show that this effect could arise from the presence of just two populations of radio source, with different properties, rather than from any systematic errors or selection effects in the data.

We postulate two different populations of radio sources with different spectral index distributions, designated 'flatter' and 'steeper'. We model these two populations as having differential source counts $\frac{dN}{dS} \propto S^b$ with $b_{\rm flat} = -1.7$ and $b_{\rm steep} = -2.5$. By normalizing the two counts in such a way that they contribute equal numbers of sources at 40 mJy, we can generate a total source count, from their sum, which is consistent with that found from our data (Fig. 16). We then assume that the flatter spectrum sources have spectral indices drawn from a Gaussian distribution with mean $\alpha_{\rm flat} = 0.2$ and $\sigma(\alpha_{\rm flat}) = 0.3$ and that the steeper spectrum sources have spectral indices drawn from a Gaussian distribution with mean $\alpha_{\rm steep} = 0.8$ and $\sigma(\alpha_{\rm steep}) = 0.3$. Using this model, we generate the spectral index distributions for flux bins $5.5 \leq S < 25$ mJy, $25 \leq S < 100$ mJy and $S \geq 100$ mJy, shown in Fig. 17, and see that they correspond to the distributions derived from the data, shown in Fig. 13.

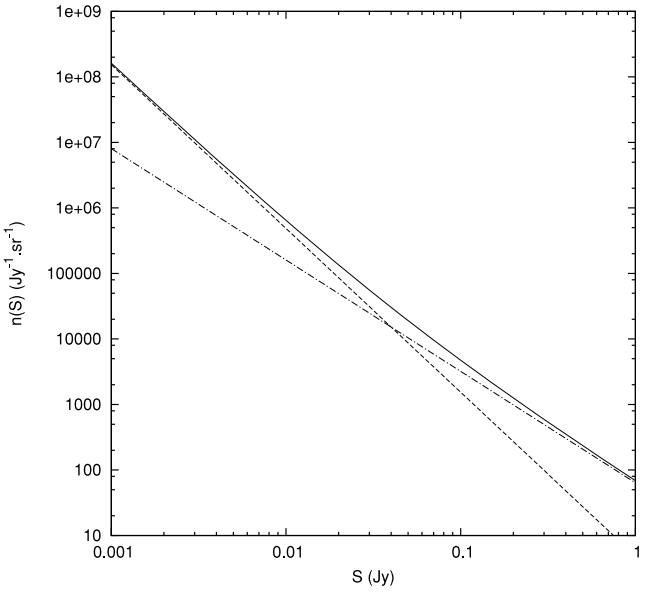

Figure 16. Simulated source counts generated from a model of two populations of radio sources which follow power-law source counts. The dot–dashed line corresponds to the flatter spectrum sources, the dashed line to the steeper spectrum sources and the solid line to the total source population for this model.

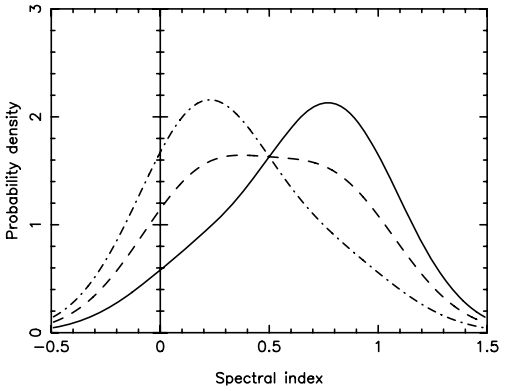

Figure 17. Simulated spectral index distributions generated from a model of two populations of radio sources. The solid line shows the spectral index distribution for sources in the flux density range $5.5 \leq S < 25$ mJy, the dashed line for sources in the flux density range $25 \leq S < 100$ mJy and the dot–dashed line for sources $S \geq 100$ mJy. These simulations correspond to the results shown in Fig. 13.

We stress that this is a very much oversimplified model, but it serves to demonstrate that a significant shift in the spectral index distribution, over a range of two orders of magnitude in flux density, is physically plausible. We expect that the spectral index distribution of a sample of sources selected at low frequency, e.g. 1.4 GHz, will show a much smaller variation with flux density, owing to the smaller proportion of flat spectrum sources in such a sample. This expectation appears consistent with the spectral index distribution between 1.4 and 30 GHz, for a sample selected at 1.4 GHz, observed by Mason et al. (2009).

9 CONCLUSIONS

(i) By developing our techniques of observation and analysis, we have succeeded in extending the 9C survey to a completeness

limit of ≈10 mJy in an area of 115 deg^2 and of ≈5.5 mJy in an area of 29 deg^2. As a blind survey at 15.2 GHz to this depth, it provides a unique resource for the study of the extragalactic source population at high radio frequency. It is particularly valuable for the investigation of the foreground point-source contamination in CMB observations, not only for the VSA but also for a wide range of other CMB experiments.

(ii) We have extended the 15-GHz differential source count to 5.5 mJy and detect no evidence of a change from the fitted power law calculated in Paper I: $n(S) = 51(S/\mathrm{Jy})^{-2.15}\,\mathrm{Jy}^{-1}\,\mathrm{sr}^{-1}$. Comparing our normalized count $S^{2.5}n(S)$ with that derived from the model of de Zotti et al. (2005), we find that our count appears to lie significantly below their prediction in the lower flux density range.

(iii) We have correlated our 15-GHz source lists with NVSS at 1.4 GHz and selected flux-limited samples at both 15 and 1.4 GHz. We find, as expected, that the 15-GHz samples contain a higher proportion of sources with flat and rising spectra than the 1.4 GHz samples. Also, in the 15-GHz samples, the proportion of such sources increases significantly with increasing flux density. These results, and the fact that more than 4 per cent of the sources below 10 mJy at 15 GHz do not appear in NVSS, illustrate the problems inherent in using a low-frequency catalogue to characterize the source population at a much higher frequency.

10 FUTURE WORK

We see that all our results are relevant to the estimation of extragalactic source populations at high radio frequencies and of the consequent effects of foreground sources on CMB observations. In particular, there is the problem of the so-called 'CBI excess' (Mason et al. 2003), which is the apparent existence of an excess of power over intrinsic CMB anisotropy on small angular scales ($l > 2000$). The question of whether this can be ascribed to contamination from the point-source foreground is discussed fully in Mason et al. (2009) and Sievers et al. (2009).

We intend to collaborate with Mason et al. to explore further the comparison of the results in their paper (2009) with ours here and, if possible, to follow up our deeper source list with simultaneous observations at 15 and 30 GHz. Since 9C is so close in frequency, this should provide more useful information on the deep source counts at 30 GHz which are critical for interpreting the CBI excess.

The RT has now been reconfigured and upgraded to form the Large Array of the Arcminute Microkelvin Imager (Zwart et al. 2008). This instrument can reach the same flux density levels as the RT in times of about two orders of magnitude shorter, enabling us to undertake even deeper surveying at 15 GHz.

ACKNOWLEDGMENTS

We are indebted to the staff of the Mullard Radio Astronomy Observatory for the operation of the RT, which was funded by PPARC. We are grateful to Dave Green for his input to this work and to Sally Hales for managing the online catalogues. MLD acknowledges an STFC studentship.

REFERENCES

Becker R. H., White R. L., Helfand D. J., 1995, ApJ, 450, 559
Bolton R. C. et al., 2004, MNRAS, 354, 485
Bolton R. C., Chandler C. J., Cotter G., Pearson T. J., Pooley G. G., Readhead A. C. S., Riley J. M., Waldram E. M., 2006a, MNRAS, 367, 323
Bolton R. C., Chandler C. J., Cotter G., Pearson T. J., Pooley G. G., Readhead A. C. S., Riley J. M., Waldram E. M., 2006b, MNRAS, 370, 1556
Cleary K. A. et al., 2005, MNRAS, 360, 340
Cleary K. A. et al., 2008, MNRAS, 386, 1759
Condon J. J., Cotton W. D., Greisen E. W., Yin Q. F., Perley R. A., Taylor G. B., Broderick J. J., 1998, AJ, 115, 1693
de Zotti G., Ricci R., Mesa D., Silva L., Mazzotta P., Toffolatti L., Gonzalez-Nuevo J., 2005, A&A, 431, 893
Gawroński et al., 2009, preprint (arXiv:0909.1189)
Kellermann K. I., Pauliny-Toth I. I. K., 1968, ARA&A, 6, 417
Kellermann K. I., Pauliny-Toth I. I. K., Davis M. M., 1968, Astrophys. Lett., 2, 105
Mason B. S. et al., 2003, ApJ, 591, 540
Mason B. S., Weintraub L. C., Sievers J. L., Bond J. R., Myers S. T., Pearson T. J., Readhead A. C. S., Shepherd M. C., 2009, ApJ, 704, 1433
Massardi M. et al., 2008, MNRAS, 384, 775
Murphy T. et al., 2010, MNRAS, in press (arXiv:0911.0002)
Peacock J. A., Wall J. V., 1981, MNRAS, 194, 331
Ricci R. et al., 2004, MNRAS, 354, 305
Riley J. M., Green D. A., 1998, MNRAS, 301, 417
Sadler E. M. et al., 2006, MNRAS, 371, 898
Sadler E. M., Ricci R., Ekers R. D., Sault R. J., Jackson C. A., de Zotti G., 2008, MNRAS, 385, 1656
Sievers J. L. et al., 2009, preprint (arXiv:0901.4540)
Skrutskie M. F. et al., 2006, AJ, 131, 1163
Taylor A. C. et al., 2003, MNRAS, 341, 1066
Voges W. et al., 1999, A&A, 349, 389
Waldram E. M., Bolton R. C., Pooley G. G., Riley J. M., 2007, MNRAS, 379, 1442
Waldram E. M., Pooley G. G., Grainge K. J. B., Jones M. E., Saunders R. D. E., Scott P. F., Taylor A. C., 2003, MNRAS, 342, 915 (Paper I)
Watson R. A. et al., 2003, MNRAS, 341, 1057
Wilkinson P. N., Browne I. W. A., Patnaik A. R., Wrobel J. M., Sorathia B., 1998, MNRAS, 300, 790
Zwart J. T. L. et al., 2008, MNRAS, 391, 1545

SUPPORTING INFORMATION

Additional Supporting Information may be found in the online version of this article:

Table 4. The source catalogue.

Please note: Wiley-Blackwell are not responsible for the content or functionality of any supporting materials supplied by the authors. Any queries (other than missing material) should be directed to the corresponding author for the article.

This paper has been typeset from a TEX/LATEX file prepared by the author.